Deformation structures in the frontal prism near the Japan Trench: Insights from sandbox models

Santanu Bose, Puspendu Saha, James J Mori, Christie Rowe, Kohtaro Ujiie, Frederick M Chester, Marianne Conin, Christine Regalla, Jun Kameda, Virginia Toy, et al.

Deformation structures in the frontal prism near the Japan Trench: insight from Sandbox Models

Santanu Bose[1*], Puspendu Saha[1], James J. Mori[2], Christie Rowe[3], Kohtaro Ujiie[4], Frederick M. Chester[5], Marianne Conin[6], Christine Regalla[7], Jun Kameda[8], Virginia Toy[9], James Kirkpatrick[10], Francesca Remitti[11], J. Casey Moore[12], Monica Wolfson-Schwehr[13], Yasuyuki Nakamura[14], Anchit Gupta[15]

[1]University of Calcutta, Department of Geology, Experimental Tectonic Laboratory, 35 Ballygunge Circular Road, Kolkata-700 019 India
[2]Earthquake Hazards Division, Disaster Prevention Research Institute, Kyoto University Gokasho, Uji Kyoto 611-0011 Japan
[3]Earth and Planetary Sciences Department, McGill University, 3450 University Street, Montreal, QC H3A 0E8 Canada
[4]Graduate School of Life and Environmental Sciences, University of Tsukuba, 1-1-1 Tennodai,Tsukuba 305-0006 Japan
[5]Center for Tectonophysics, Department of Geology and Geophysics, Texas A&M University, College Station TX 77843-3115 USA
[6]EA4098 LaRGE, Université des Antilles et de la Guyane, Pointe-à-Pitre, France.
[7]Department of Geosciences, The Pennsylvania State University, University Park PA 16802 USA
[8] Department of Natural History Sciences, Faculty of Science, Hokkaido University, Sapporo 060-0810, Japan
[9]Department of Geology, University of Otago, 360 Leith Walk, Dunedin 9054 New Zealand
[10]Department of Geosciences, Colorado State University, Fort Collins, Colorado, USA
[11]Dipartimento di Scienzedella Terra, Università di Modena e Reggio Emilia largo, S. Eufemia, 19 41100 Modena Italy
[12]Department of Earth and Planetary Sciences, University of California Santa Cruz, 1156 High, St., Santa Cruz, CA 95064 USA
[13]Center for Coastal and Ocean Mapping, Joint Hydrographic Center, University of New Hampshire, 24 Colovos Road, Durham NH 03824 USA
[14]Institute for Research on Earth Evolution, JAMSTEC, Yokohama, Japan
[15]Department of Earth Sciences,Indian Institute of Technology, Roorkee- 247667, Uttarakhand India

*Correspondence to: bose.santanu@gmail.com

Abstract

We have used sandbox experiments to explore the mechanics of the frontal prism structures documented by new borehole and seismic reflection data from IODP Expedition 343 (JFAST). This study investigated the effects of down-dip (across

47 trench axis) variations in frictional resistance along a decollement on the structural
48 development of frontal wedges near subduction zones. To clarify our understanding
49 on the wedge growth over horst-and-graben structures in the subducting plate near the
50 Japan Trench, we performed sandbox experiments with alternate zone of relatively
51 high and low friction on the basal decollement. Our experiments verify that high
52 frictional resistance on the basal fault is needed to produce the observed internal
53 deformation and fault-and-fold structures in the core samples collected during JFAST.
54 Varying down-dip frictional resistance along the decollement causes a temporal
55 change in the style of internal deformation within the wedge and often gives rise to
56 two distinctive structural domains, separated by a break in the surface slope of the
57 wedge: (i) complexly deformed inner wedge with steep surface slope and (ii) shallow
58 taper outer wedge, characterized by a sequence of imbricate thrusts. Our experiments
59 further demonstrate that the topographic slope-break in the wedge develops when the
60 hinterland part of the wedge essentially stops deforming internally, leading to in-
61 sequence thrusting with the formation of outer wedge with low taper angle. For a
62 series of alternate high and low frictional conditions on the basal fault the slope of the
63 wedge varies temporally between topographic slope-break and uniformly sloping
64 wedge.

65 *Keywords*: sandbox experiments, inner and outer wedge, slope-break, horst-and-
66 graben structure, fault friction

67

68 **1. Introduction**

69 It is now well known that the subduction of bathymetric features in the oceanic
70 plate, e.g., seamounts, aseismic ridges, volcanic plateaus has a strong influence on the
71 development of diverse morphological features and deformation structures in the

overriding plate (Domingues et al., 2000; Malavieille, 1984; von Huene and Culotta, 1989; von Huene and Lallemand, 1990; Lallemand et al., 1992; Lallemand et al., 1994; von Huene et al., 2004; Park et al., 1999; Wang and Hu, 2006). However, their studies indicate that the styles of deformation in the overriding plate vary with the geometry of bathymetric features in the subducting plate. For example, the subduction of seamounts develops steeper surface slope in the inner wedge than that in the outer wedge (Park et al., 1999; Domingues et al., 2000). On the contrary, the subduction of aseismic ridges develops steep outer wedge slope associated with almost flat inner wedge (Lallemand et al., 1992). Despite dominance of horst-and-graben structure at most trenches, its influence on frontal wedge growth has still remained relatively unexplored. We therefore focus the present work to analyze the impacts of subducted horst-and-graben structures on the evolution of frontal wedge near the Japan Trench.

Geophysical investigations along several sections across the Japan Trench (Fig. 1b and c) recorded a series of horst-and-graben structures on the subducting plate beneath the frontal wedge (Tsuru et al., 2002; Kodaira et al., 2012; Nakamura et al., 2013). Moreover, earlier studies have shown that the sediment thickness in the incoming Pacific plate near the Japan Trench is thin and the thinning of sediment cover mostly occurs above the horst block (Groshong, 2006). The combination of the effects of the differences in sediment thickness and surface roughness over horst-and-graben structure in the subducting plate cause varying degrees of coupling at the plate interface, creating varying frictional properties on the decollement (Pacheco et al., 1993; Tanioka et al., 1997; von Huene et al., 1999; Bilek, 2007; Das and Watts, 2009). In the present study we have used sandbox experiments to simulate the effects of down-dip variations in the frictional strength on the basal decollement to investigate the structural development of frontal wedge and finally, provide a

97 mechanical model for explaining the structural evolution of frontal wedge over horst
98 and graben structure near the Japan Trench.
99 Integrated Ocean Drilling Program (IODP) Expedition 343 (JFAST) drilled to a
100 depth of 836 meters below seafloor (mbsf) near the Japan Trench at site C0019
101 through the plate boundary fault zone over the horst block, located about ~ 6 km
102 westward from the trench axis (Fig. 1a). Core samples collected during the expedition
103 have provided a great opportunity to compare our experimental results with the
104 observed deformation structures within the frontal wedge (Chester et al., 2013,
105 Kirkpatrick et al., 2014). Borehole data and associated seismic images provide new
106 structural information that has been modeled in this study to show the effects of
107 friction on the megathrust near the Japan Trench.
108 .
109 **2. Experimental methods and materials**
110 Sandbox experiments have proved to be useful in understanding the mechanics
111 of thin-skinned accretionary wedges using the concept of critical taper theory
112 (Chapple, 1978; Boyer and Elliot, 1982; Davis et al., 1983; Dahlen, 1990). The angle
113 of critical taper is defined by the summation of basal inclination (β) and surface slope
114 (α). According to critical taper model, a wedge deforms internally and thereby,
115 increases its taper and at a critically tapered angle the wedge develops internal
116 stresses, leading the wedge on the verge of failure. At this stage, shear stress at the
117 base reaches a value that assists frictional sliding at the decollement (Davis, 1983;
118 Boyer and Elliot, 1982). Theoretically and experimentally it has been shown that the
119 angle of critical taper is proportional to the frictional condition on the basal
120 decollement according to the following equation (Dahlen, 1990):

121 $$\alpha + \beta = (\beta + \mu_b)\left(\frac{1-\sin\phi_c}{1+\sin\phi_c}\right) \quad (1)$$

122

123 where, μ_b is the coefficient of static friction on the decollement and ϕ_c is the angle of
124 internal friction of the frontal prism material.

125 In the present study, we have prepared our experimental models over varying
126 down-dip frictional conditions on the decollement to simulate the effect of horst-and-
127 graben structure along the basal decollement (Fig.2). We have considered relatively
128 higher frictional coefficient on the decollement above the horst block because of its
129 enhanced surface irregularities due to little or no sediment cover, leading to a strong
130 coupling with the overriding plate than that over the graben sediments. Thus the horst
131 and graben structure gives rise to alternate zones of relatively strong and a weak
132 contact respectively with the overriding plate on the decollement. In the laboratory
133 scaled experiments the higher basal friction (μ_b= 0.46), simulating the decollement
134 immediately above the horst block, was achieved by pasting commercial sand paper
135 (P30, average grit size 622.0 microns) on a glass plate and a relatively lower basal
136 friction (μ_b = 0.36) was obtained by sieving a veneer of boric acid powder (0.001mm
137 beads) over the glass plate in order to model the frictional strength above the graben
138 sediments. However, in some experiments we pasted rigid block of 5mm thick acrylic
139 sheet over the basal glass plate to model the horst block. However, in the second set
140 of experiments, we had to stop the experiment once the buttress reached the edge of
141 the acrylic block. Experimental results from these two different sets of experiments,
142 however, show that frontal wedge propagation ceases once the decollement
143 propagation reaches the high frictional patch / edge of the rigid acrylic sheet (see
144 electronic supplementary Fig. S1). This finding suggests that the use of high frictional

145 patch on the basal glass plate is a suitable analog for simulating natural horst-block.
146 The advantage of using sandpaper over rigid block is that the hinterland buttress can
147 override the high frictional patch without limiting the amount of shortening during the
148 experimental run.

149 In the model setup, Zone I represents a graben in the seismogenic plate interface
150 and Zone II corresponds to a horst block in the subducting plate (Fig. 2). Although a
151 majority of our experiments were carried out with one high frictional patch between
152 zones of relatively lower friction on the basal fault, a few experiments were carried
153 out with two zones of high frictional patches to understand the effects of a series of
154 horst-and-graben structures. Experimental models were prepared by sieving sand
155 layers from a constant height of 20 cm in a rectangular glass-walled sandbox
156 apparatus over a rigid base of varying basal friction (μ_b) (Fig. 2). The length and
157 width of the apparatus are 110 cm and 35 cm respectively. The model width was more
158 than fifteen times its thickness to avoid the effects of friction at the interface of sand
159 layers and the glass sidewalls (Souloumiac et al., 2012). The coefficients of basal
160 friction (μ_b) were calculated separately from sliding experiments using dry non-
161 cohesive sand. Note that the values of μ_b used in our experiments are merely imposed
162 qualitatively for simulating natural situation that do not claim the exact values for
163 natural analogue. The glass walls of the sandbox were cleaned and dried carefully to
164 remove surface moisture. This process is important in order to prevent sticking of
165 sand to the glass walls. Experiments were carried out in controlled laboratory
166 conditions to avoid the influence of atmospheric moisture contents.

167 We used dry, non-cohesive natural quartz-rich (>90%) sand, texturally matured
168 with well rounded grains (average sphericity of 0.8), as analogue material for scaled
169 model experiments simulating crustal scale brittle deformation (Davis et al., 1983;

170 Mulugeta, 1988; Koyi, 1995; Mandal et al., 1997; Schellart, 2000). The sand material
171 had a bulk density of 1600 kg/m^3, and a coefficient of internal friction close to 0.57.
172 Our model scales to nature with a ratio of 2.7x10^{-5}, where 1 cm in the model is
173 equivalent to 360 m in nature (Table 1). The cohesion of model material (dry quartz
174 sand) in our experiment is around 20 Pa, which scales to 2 MPa (Gutscher et al.,
175 1998) for unconsolidated marine sediments (Hoshino et al., 1972). The models were
176 deformed in a pure shear box at a uniform velocity of 5 mm / minute using a
177 computer controlled step-up motor by setting a backstop at the rear of the sand layers.
178 Previous studies revealed that buttress geometry is important in the development of
179 wedge geometry in sand layers (Byrne et al., 1988; Persson and Sokoutis, 2002).
180 However, we used planar vertical buttress in our experimental setup in order to model
181 a mono-vergent accretionary wedge observed in the Japan Trench (Mulugeta, 1988;
182 Storti and McClay, 1995; Gutscher et al., 1998; Bose et al., 2009). Although sand
183 layer of 1cm thickness should have been used in our experiments according to the
184 scaling law, we have exaggerated the thickness of sand layers to 2 cm in all
185 experiments for obtaining better resolution of deformation structures as well as to
186 understand the deformation mechanism clearly during the experimental run. However,
187 we ran experiments with sand layers of 1 cm thickness to verify the influence of
188 model thickness in experimental results. These experiments show broad resemblance
189 in the first order geometry of the wedge (see electronic supplementary Fig. S2) and
190 therefore validates the use of 2 cm thick sandlayers in the model experiments. During
191 the experimental run, we photographed through the lateral glass wall continuously
192 after an interval of 5 seconds, keeping the camera at a fixed distance from the model.
193 Model deformations were analyzed from successive photographs taken during the
194 experimental run.

195

196 **3. Experimental Results**

197 Our experiments suggest that the frontal wedge near the Japan Trench has
198 evolved over varying down-dip frictional condition on the decollement during
199 subduction of horst-and-graben. In our experiments, the wedge started to grow above
200 Zone I by in-sequence thrusting at the *initial stage* and developed a gentle surface
201 slope (α) at uniform shortening rate (Figs. 3b-3c, 4a). The vertical growth of the
202 wedge at the backstop attained an almost stationary value when the model was
203 shortened by 5 cm in all experiments (Fig. 4b). At this stage, the frontal propagation
204 of the wedge dominated over the vertical growth through sequential thrusting until the
205 deformation front reached Zone II. During this stage the wedge developed a critical
206 taper, α equals 7.5° (Figs. 3d, 4a), which is closer to the theoretical value of surface
207 slope (α) of 6° obtained from "equation 1" for $\beta = 0$, $\mu_b = 0.36$ and $\phi_c = 0.57$.
208 However, the overestimation of α in the experimental result is self-consistent.

209 The mode of internal deformation and its geometry changed completely when
210 the decollement propagation reached the edge of high frictional patch (Zone II, μ_b=
211 0.42), simulating a horst (Fig. 3e, see electronic supplementary Figs. S1 A [d] and B
212 [d]). At this stage, decollement propagation ceased and the wedge formed over Zone I
213 started deforming internally by increasing the wedge height consistently, developing a
214 steep topographic slope (Fig. 4). This stage of wedge growth has been defined as
215 *intermediate stage* (Figs. 3e-3f). The topographic slope of the wedge at this stage
216 became much higher than the predicted value from "equation 1", leading the wedge to
217 grow to a super critical state. It is likely that the cessation of decollement propagation
218 promotes the development of supercritical wedge in order to accommodate the
219 amount of horizontal shortening, and eventually facilitates slope failure (Fig. 3f).

220 During this stage experimental models demonstrated mechanical rotation and
221 reorientation of already deformed sand layers in the hanging wall, giving rise to a
222 complex deformation structures within the deforming wedge.
223 With further horizontal shortening, the deformation front crossed the Zone II
224 and propagated onto the region above zone I over low μ_b, simulating another graben,
225 by the process of in-sequence thrusting and eventually, developed a separate wedge
226 with a low angle of taper as expected to occur over low basal friction. Such spatial
227 and temporal variations in the style and intensity of deformation across the wedge
228 finally gave rise to distinct topographic slope-break in the wedge geometry separating
229 the steep inner wedge from the low tapered outer wedge (Figs. 3g-3h and 4a). During
230 the growth of outer wedge, the internal deformation in the inner wedge completely
231 stopped (Fig. 4b) and the horizontal shortening was entirely accommodated by in-
232 sequence thrusting over weak fictional base. For simplicity in description, we describe
233 this stage of wedge growth as *final stage*, which characterizes the development of
234 topographic slope-break with the cessation of internal deformation within the inner
235 wedge. Experiments with varying width of Zone II showed that increasing the width
236 of the Zone II (e.g. 30 cm) required large amount of shortening for the development
237 of the topographic slope-break (Figs. 5 and 4, see electronic supplementary Fig. S3).
238 The development of slope-break in the wedge geometry thus can be treated as a
239 potential indicator for interpreting long term frictional condition on the decollement.
240 Experiments with more than one high frictional patch (Zone II) on the basal
241 fault showed that the surface slope of outer wedge (e.g., the wedge over low μ_b) was
242 increasing progressively with ongoing shortening once the decollement propagation
243 was again resisted by another high frictional patch in the front. As a consequence, the
244 wedge geometry was completely modified along with the destruction of topographic

slope-break (Fig. 6h). With further shortening the outer wedge progressively merged with the inner wedge, giving rise to a single wedge with steep uniform surface slope (Fig. 6i). During this process of wedge modification, the inactive inner wedge again resumed to deform by mechanically rotating all preexisting structures and thereby, increasing the complexity of deformation structures towards the hinterland part of the wedge (Fig. 6i, 6k). With continuous shortening, the deformation within this steep wedge completely stopped once the deformation front propagated over another low frictional base in the front with the onset of the development of new outer wedge by in-sequence thrusting (Figs. 6j, 6k). Based on above results, it is evident that the geometry of the frontal wedge is essentially transient with varying down-dip frictional strength on the decollement in tectonically active convergent belts over long time scale.

4. Discussion

4.1 *Implication of varying down-dip basal friction*

On the basis of the above observations and interpretations on the experimental results we discuss below the role of basal friction in the structural development of frontal wedge near the Japan Trench. Our study reveals that varying down-dip frictional strength on the decollement causes a drastic change in the wedge taper, giving rise to a steep *inner wedge* and gentle *outer wedge*. This lateral change in the surface slope across the wedge separates the entire wedge into two distinctive structural domains: (i) complex internal deformation within *the inner wedge* and (ii) the *outer wedge* is deformed mostly by sequential thrusting. Experimental results show that the growth of the inner wedge begins by in-sequence thrusting over low frictional base following the model of critical angle of taper (Davis et al., 1983;

Mulugeta, 1988; Koyi, 1995; Gutscher et al., 1998; Yamada et al., 2006; Bose et al., 2009). However, with ongoing shortening the taper angle of the wedge progressively steepens with the termination of decollement propagation by the increased frictional resistance along the decollement. The steepening of the wedge slope couple with intense internal deformation within it continues until the deformation front crosses from the zone of high to low friction on the basal decollement. The progress of the deformation front over the lower frictional base immediately stops internal deformation within the deformed wedge (Figs. 3g- 3h) and thereby, initiates a renewed phase of in-sequence thrusting in response to continuing horizontal shortening, leading to the development of shallow taper outer wedge. This process of wedge propagation over varying basal friction gives rise to the development of topographic slope-break between the inner and the outer wedges. The characteristic geometry of the slope-break in the tectonic wedge becomes prominent when the wedge front continues to deform over a uniform low frictional base for large horizontal shortening (Fig. 5a-g).

4.2 *Interpretation of wedge development near the Japan Trench*

The present study has an important implication in understanding the development of frontal wedge near the Japan Trench. Seismic sections across the Japan Trench show that the slope of the frontal prism over horst-and-graben structure changes from 10° in the landward part to 4° towards the trench (Fig. 1b). Comparing our experimental results with seismic data from frontal wedge near the Japan Trench suggest that the varying down-dip frictional strength along the basal decollement caused the present geometry of the wedge and deformation structures within it near the Japan Trench (Fig. 1b and 1c). Our experimental results suggest that the subduction of horst-and-graben structure near the Japan Trench are potential factors

295 for creating varying degree of coupling with the overriding plate that eventually
296 developed the characteristic topographic slope-break. It further reveals that the inner
297 wedge with steep slope over the horst block must have formed prior to the
298 propagation of deformation front over the graben sediments. Our experimental study
299 shows that initiation of growth of the outer wedge over low basal friction deactivates
300 the internal deformation of the inner wedge. This has led to infer that the present day
301 plate convergence near the Japan Trench is accommodating entirely by in-sequence
302 thrusting over the low friction graben sediments. Previous experimental findings
303 (Huiqi et al., 1992; Bose et al., 2009) along with the present study indicate that the
304 occurence of a series of imbricate thrusts over graben sediments, preserved in the
305 outer wedge of the Japan Trench (Kodaira et al., 2012; Nakamura et al., 2013), have
306 formed over relatively weak decollement (Figs. 7c).
307 The structural interpretations from the drill core samples collected during
308 JFAST and seismic data reveal that the frontal prism lying over the subducted horst
309 block (~ high frictional patch) is structurally chaotic, which is also consistent with the
310 observed deformation structures in our experimental models. The dip of beds
311 measured in the core samples varies from 20° to 80° and they are also traversed by
312 numerous closely spaced core scale faults (Chester et al., 2013; Nakamura et al.,
313 2013; Kirkpatrick, 2014) (Fig. 7). Our experimental results show that the complexity
314 in the internal deformation within the inner wedge increases with the onset of
315 steepening of inner wedge slope when the frontal propagation of the decollement is
316 resisted by the high frictional patch during ongoing shortening (Figs. 3 and 4). This
317 has led to infer that the variably steeply dipping beds in the core samples might have
318 evolved through the process of mechanical rotation of earlier structures within the
319 hanging wall when the decollement propagation was either temporarily stopped or

was very slow due to high-frictional resistance along the horst block. Based on above discussions, it appears that subduction of horst-and-graben structure played a crucial role in increasing the complexity of deformation structures observed at the drill site near the Japan Trench. With continued plate convergence over time the deformation front eventually crossed the high frictional patch resulting the break in the surface slope observed between the inner and outer wedges in the frontal prism. In the laboratory experiments, the break in the surface slope of the wedge becomes prominent once the backstop overrides the high frictional patch and consequently, develops outer wedge by in-sequence thrusting (Figs. 3g, 6f and 6j). Comparing our experimental results with seismic images reveal that the buttress (~ backstop in the experimental setup) in the natural situation near the Japan Trench currently lies on the west of the JFAST drilling site towards landward part of the wedge, as also predicted by earlier workers (Tsuru et al., 2002) (Fig. 7b and 7c). Our experimental results further reveal that the observed slope sediments between the inner and outer wedge in the Japan Trench might have accumulated during the growth of supercritical wedge as identified in the *intermediate stage* in experiments and the sediment accumulation continued until the deformation front crossed the horst block (Fig. 3f). This, however, does not rule out the possibility of rotational slumping of the slope sediments at the frontal wedge by later reactivation during the 2011 megaearthquake event (Strasser et al., 2013).

The present experimental study has also predicted why there is lack of natural examples of the occurrence of multiple slope-breaks in accretionary prisms. Experiments with two high frictional patches show that the cessation of the propagation of outer wedge by another zone of high frictional patch in the front modifies the wedge geometry thoroughly by mechanical rotation of all pre-existing

deformation structures including the zone of topographic slope-break, forming a wedge with a uniformly steep surface slope (Fig. 6). These observations have led to infer that the subduction of the horst block in the Pacific plate lying currently on the east of the Japan Trench will eventually modify the present wedge geometry having a topographic slope –break to a uniformly steep slope.

5. **Conclusion**:

Our main conclusions are as follows:

1) Down-dip frictional variations on the decollement cause temporal and spatial variations in the geometry of the frontal wedge.
2) Surface slope-break develops when the deformation front crosses from high to low basal friction. The break in the surface slope separates the entire wedge into two distinct structural domains: inner and outer wedges.
3) The inner wedge is characterized by steep wedge slope and complex internal structures, whereas the outer wedge is deformed by in-sequence thrusting, leading to shallow taper angle.
4) The experimental models thoroughly explain the structural evolution of the frontal wedge near the Japan Trench observed in seismic images and borehole data.
5) We interpret that the complexity of internal deformation observed in core samples and localization of steep surface slope towards the landward part of the wedge near the Japan Trench is caused by the cessation of decollement propagation by the horst block in the subducting plate lying beneath JFAST drill site.

6) The development of shallow taper outer wedge over the graben sediments by in-sequence thrusting marks the cessation of internal deformation in the rear part of the wedge (~ inner wedge), creating the topographic slope-break near the Japan Trench.

Acknowledgement: We thank scientific and drilling staff on Drilling Vessel *Chikyu* for their constant assistance during the IODP expedition 343. We thank Ylona van Dinther and Marc-Andre Gutscher for their insightful reviews and constructive suggestions for improvement of this work. We also thank W.P. Schellart for his guideline to revise the manuscript. The work is supported by MOES, Govt. of India and DST, Govt. of India grants to SB and PS acknowledge CSIR, India for financial support.

References

Bilek,S., 2007. Influence of Subducting Topography on Earthquake Rupture In:T. Dixon and C.Moore(eds.), The Seismogenic Zone of Subduction Thrust Faults, ColumbiaUniversityPress.123.

Bose, S., Mandal,N., Mukhopadhyay,D.K., Mishra,P. 2009. An unstable kinematic state of theHimalayan tectonic wedge: Evidence from experimental thrust-spacing patterns. J. Struct. Geol., 31,83-91.

Boyer, S.E., Elliot, D., 1982.Thrustsystems. Am. Assoc. Pet. Geol.. 67,1196-1230.

Byrne, D.E., Davis D.M., Lynn, R.S., 1998.Loci and maximum size of thrust earthquakes and the mechanics of the shallow region of subduction zones. Tectonics, 7, 833.

Chapple, W.M., 1978.Mechanics of thin-skinned fold-and-thrust belts. Geol. Soc. Am. Bull.89,1189.

Chester, F.M., Rowe, C., Ujiie, K., Kirkpatrick, J., Regalla, C., Remitti,

400 F.,Moore, J.C., Toy, V., Wolfson-Schwehr, M., Bose, S., Kameda, J., Mori,
401 J.J., Brodsky, E.E., Eguchi, N., Toczko, S., Expedition 343 and 343T
402 Scientists.Structure and composition of the plate-boundary slip zone for the
403 2011 Tohoku-Oki earthquake. Science 342, 1208-1211.

404 Dahlen,F.A., 1990. Critical Taper Model of Fold-and-Thrust Belts and
405 Accretionary Wedges.Annu.Rev.EarthPlanet.Sci.18,55-99.

406 Das, S., Watts, A.B., 2009. Effects of subducting seafloor topography on the
407 rupture characteristics of great subduction zone earthquakes. In:S.
408 Lallemandand F. Funiciello(eds.), Subduction Zone Geodynamics,
409 Springer-Verlag Berlin Heidelberg 103-118.

410 Davis, D.M., Suppe, J., Dahlen, F.A., 1983. Mechanics of fold-and-thrust belts
411 and accretionary wedges. J. Geophys. Res. 88, 1153-1172.

412 Dominguez, S., Malavieille, J., Lallemand, S.E., 2000. Deformation of
413 accretionary wedges in response to seamount subduction: Insights from
414 sandbox experiments. Tectonics. 19, 182-196.

415 Groshong, R.H., 2006. 3-D Structural geology: a practical guide to quantitative
416 surface and surface map interpretation. Springer, New York, p 400.

417 Gutscher, M. A., Kukowski, N., Malavieille, J., Lallemand, S., 1998. Material
418 transfer in accretionary wedges from analysis of a systematic series of
419 analog experiments. J. Struct. Geol. 20(4), 407-416.

420 Hoshino, K ., Koide, H., Inmni, K., lwamuraa, S., Mitsui, S., 1972. Mechanical
421 properties of Japanese teritary sedimentary rocks under high confining
422 pressures., Geol. Surv. of Jpn, Kawasaki, Japan, p 200.

423 Huiqi, L., McClay, K. R., Powell, D. 1992. Physical models of thrust wedges. In
424 Thrust tectonics. Springer Netherlands, 71-81.

425 Kirkpatrick, J. D., Rowe, C. D., Ujiie, K., Moore, J. C., Regalla, C., Remitti, F.,
426 Toy, V., Wolfson-Schweh, M., Kameda, J., Bose, S., Chester, F. M., 2014.
427 Structure and lithology of the Japan Trench subduction plate boundary
428 fault. Tectonics. DOI: 10.1002/2014TC003695.

429 Kodaira, S., No, T., Nakamura, Y., Fujiwara, T., Kaiho, Y., Miura, S., Takahashi,
430 N., Kaneda, Y., Taira, A., 2012. Coseismic fault rupture at the trench axis
431 during the 2011 Tohoku-oki earthquake. Nat. Geosci. 5,

doi:10.1038/NGEO1547.

Koyi, H., 1995. Mode of internal deformation of sand wedges. J. Struct. Geol.17, 293-300.

Lallemand, S. E., Schnürle, P., Malavieille, J., 1994. Coulomb theory applied to accretionary and nonaccretionary wedges: Possible causes for tectonic erosion and/or frontal accretion. J. Geophys. Res. 99, 12033-12055.

Lallemand, S. E., Malavieille, J., Calassou, S., 1992. Effects of oceanic ridge subduction on accretionary wedges: experimental modeling and marine observations. Tectonics, 11(6), 1301-1313.

Malavieille, J., 1984. Modelisation experimentale des chevauchements imbriques; application aux chaines de montagnes. Bull. Soc. Géol. Fr., (1), 129-138.

Mandal, N., Chattopadhyay, A., Bose S., 1997. Imbricate thrust spacing: experimental and theoretical analyses. In: Sengupta, S. (Ed.), Evolution of Geological Structures in Micro- to Macro-Scales. Chapman and Hall, London, 143 .

Mulugeta, G., 1988. Modeling the geometry of Coulomb thrust wedges. J. Struct.Geol.10, 847.

Nakamura, Y., Kodaira, S., Miura, S., Regalla, C., Takahashi,N., 2013. High resolution seismic imaging in the Japan Trench axis area of Miyagi, Northeastern Japan. Geophys. Res. Lett. 40, 1713-1718. doi:10.1002/grl.50364.

Pacheco,J.F.,Sykes,L.R.,Scholtz,C.H.,1993. Nature of seismic coupling along simple plateboundaries of the subduction type.J.Geophys.Res.98,14133-14159.

Park, J. O., Tsuru, T., Kaneda, Y., Kono, Y., Kodaira, S., Takahashi, N., Kinoshita, H., 1999. A subducting seamount beneath the Nankai accretionary prism off Shikoku, southwestern Japan. Geophys. Res. Lett., 26(7), 931-934.

Persson, K.S., Sokoutis, D., 2002. Analogue models of orogenic wedges controlled byerosion. Tectonophysics. 356, 323 .

Schellart, W. P., 2000. Shear test results for cohesion and friction coefficients for

different granular materials: scaling implications for their usage in analogue modelling. Tectonophysics. 324.1, 1-16.

Souloumiac, P., Mailot B., Leroy, Y.M., 2012. Bias due to side wall friction in sand box experiments, J. Struct. Geol., 35, 90 - 101.

Storti, F., McClay, K.R., 1995. Influence of syntectonic sedimentation thrust wedges in analogue models. Geology23**,** 999.

Strasser, M., Kölling, M., dos Santos Ferreira, C., Fink, H.G., Fujiwara, T., Henkel, S., Ikehara, K., Kanamatsu, T., Kawamura, K., Kodaira, S., Römer, M., Wefer, G., the R/V *Sonne* Cruise SO219A and JAMSTEC Cruise MR12-E01 scientists., 2013. A slump in the trench: Tracking the impact of the2011Tohoku- Okiearthquake.Geology.41,935-938.

Tanioka,Y., Ruff,L., Satake, K., 1997. What controls the lateral variation of large earthquake occurrence along the Japan Trench? IslandArc**.** 6,261-266.

Tsuru, T., Park, J. O., Miura, S., Kodaira, S., Kido, Y., Hayashi, T., 2002. Along‐arc structural variation of the plate boundary at the Japan Trench margin: Implication of interplate coupling. J. Geophys. Res. 107(B12), ESE-11, 1-15.

von Huene, R., Culotta, R., 1989. Tectonic erosion at the front of the Japan Trench convergent margin. Tectonophysics. 160, 75-90.

von Huene, R., Lallemand, S., 1990.Tectonic erosion along the Japan and Peru convergent margins. Geol. Soc. Am. Bull. 102. 704-720.

von Huene, R., Ranero, C. R., Vannucchi, P., 2004. Generic model of subduction erosion. Geology. 32, 913-916.

vonHuene,R.,Klaeschen,D.,Fruehn,J., 1999.RelationbetweentheSubductingPlate andSeismicityAssociatedwiththeGreat1964AlaskaEarthquake.PureAppl. Geophys.154,575.

Wang, K., Hu, Y. (2006). Accretionary prisms in subduction earthquake cycles: The theory of dynamic Coulomb wedge, J. Geophys. Res. B06410, doi:10.1029/2005JB004094.

Yamada, Y., Baba, K., Matsuoka, T., 2006. Analogue and numerical modeling of accretionary prisms with a decollement in sediments. In: Buiter, S. J. H. & Schreurs (eds) Analogue and numerical modeling of crustal- scale

processes. Geol. Soc. London Spec. Pub, 253, 169-183.

Figure Captions:

Figure 1: (a) Location map, showing the eastern coastline of Honshu, bathymetry near Japan Trench and Tohoku earthquake epicenter (red star). The yellow arrow indicates the direction of plate convergence. Inset map shows location of Expedition 343 site C0019 (red star) along seismic section Line HD 33B (Fig.1b). Line HD 26B another seismic section line shown in figure 1c. (b) Image of seismic section Line HD 33B crossing the IODP drilling site C0019 with no vertical exaggeration. It shows change in topographic slope (marked red lines) from inner wedge (~10°) to outer wedge (~ 4°) (modified after Nakamura et al., 2013). (c) Image of seismic section Line 26B with V.E. ~ 3, separated by 3.5 km from seismic line HD 33B. α_i and α_o are relative slopes of inner and outer wedges respectively, showing changes in topographic slope (modified after Nakamura et al., 2013). Pink line marks the decollement surface and blue arrow indicates the zone of topographic slope-break in both (b) and (c).

Figure 2: A sketch of the experimental setup showing 3D view of the model setup. Zones I and II represent low and high frictional contact zone respectively. Arrows on the right show the direction of shortening.

Figure 3: Progressive development of frontal wedge in sand models with 10 cm width of the Zone II. (a) Initial model, (b-e) Initial stage, (f) intermediate stage and (g-h) progressive development of wedge during the final stage (see text for details). Note that the deformation propagation towards front stopped after shortening of 14. 40 cm, but hinterland elevation continued to increase (e). 18.10 cm shortening was accommodated within the wedge, reorienting earlier structures during intermediate

stage (f). Further shortening moves the deformation front above the lower frictional base developing distinct slope-break (g-h).

Figure 4: Plots show different stages of wedge growth for varying width of zone II using high frictional patch (7 experiments) and rigid block (4 experiments). Wedge angle (a) and Wedge height at the backstop (b), are plotted as a function of actual displacement (horizontal shortening) in cm. In the initial stage of the wedge growth, wedge angle (a) and wedge height (b) reached a constant value with horizontal displacement. The intermediate stage marks the sharp increase in both wedge angle (solid line) (a) and wedge height (solid line) (b). In the final stage wedge height attained a constant value (dash line) (b) with decreasing wedge slope (dash line) (a).

Figure 5: Final stage of wedge development for varying widths of high frictional patch: 2 cm (a), 4 cm (b), 6 cm (c), 10 cm (d), 12 cm (e), 14 cm (f) and 30 cm (g). The width of the model is 35 cm for all experiments. White arrow marks the zone of topographic slope-break between inner and outer wedge.

Figure 6: Progressive development of frontal wedge growth over multiple high frictional patch, forming alternate uniform slope and topographic slope-break. (a-d) Initial stage, (e) intermediate stage with steep uniform slope, (f-g) final stage showing the development of slope-break, (h) the process of destruction of outer wedge observed in figure (g) due to another high frictional in the front, leading to steep uniform surface slope (i), (j) development of new slope-break in the wedge geometry low basal friction, (k) Plots show the variations of wedge angle (purple) and wedge elevation at the hinterland buttress (green) as a function of horizontal displacement. Note that the combination of low tapered wedge at constant wedge elevation implies growing of wedge over low frictional base (yellow shade).

Figure 7: Compilation of core data with depth at IODP sites C0019 and comparison

with experimental model. (a) Deformation unit in the core data shows variations in bedding dip with depth and three structural domains are identified. (i) upper frontal prism (0-275 mbsf) shows gently inclined bedding, (ii) lower frontal prism (276-820 mbsf) showing variable and steeply dipping beds characterized by folded and faulted sediments, (iii) base section (820 mbsf to base of the hole) with shallow to horizontal bedding represents in the footwall block in the subduction zone (modified after Chester et al., 2013). (b) Experimental model shows resemblance in the changes of bedding orientations with depth. Green arrows show the region in the experimental model comparable with core data set. White dash line in the model replicates the drilling site C0019 shown in Fig. 7c. (c) Details and interpretations of seismic image along section HD 33B.Vertical Exaggeration = 2:1 (Modified after Kodaira et al., 2012). Note that experimental model closely reproduces geometrical and structural features observed in seismic image. Both experimental and seismic section show that surface slope of the inner wedge is steeper than that of the outer wedge. Imbricate thrusts are prominent within the outer wedge. The blue arrow marks the zone of topographic slope-break between inner and outer wedges in Figs. 7b and 7c.

Table 1
Modeling Parameters and material properties

Parameter and model properties	**Sand (analogue model)**	**Natural ptototypes**	**Ratio: model/nature**
Length, L (m)	0.01	360	$\lambda = 2.7 \times 10^{-5}$
Density (kg m^{-3})	1600	2700	$\delta = 0.59$
Internal friction angle, ϕ (°)	~ 30	30 - 40	1- 0.75
Cohesion (Pa)	20	2×10^{6}	1×10^{-5}
Gravity, g (m s^{-2})	9.8	9.8	$\gamma_g = 1$
Deviatoric Stress * ($\sigma = \delta \, . \, g \, . \, L$)	157 Pa	$9.5 . 10^{6}$	16.5×10^{-6}

* Based on Schellart, 2000

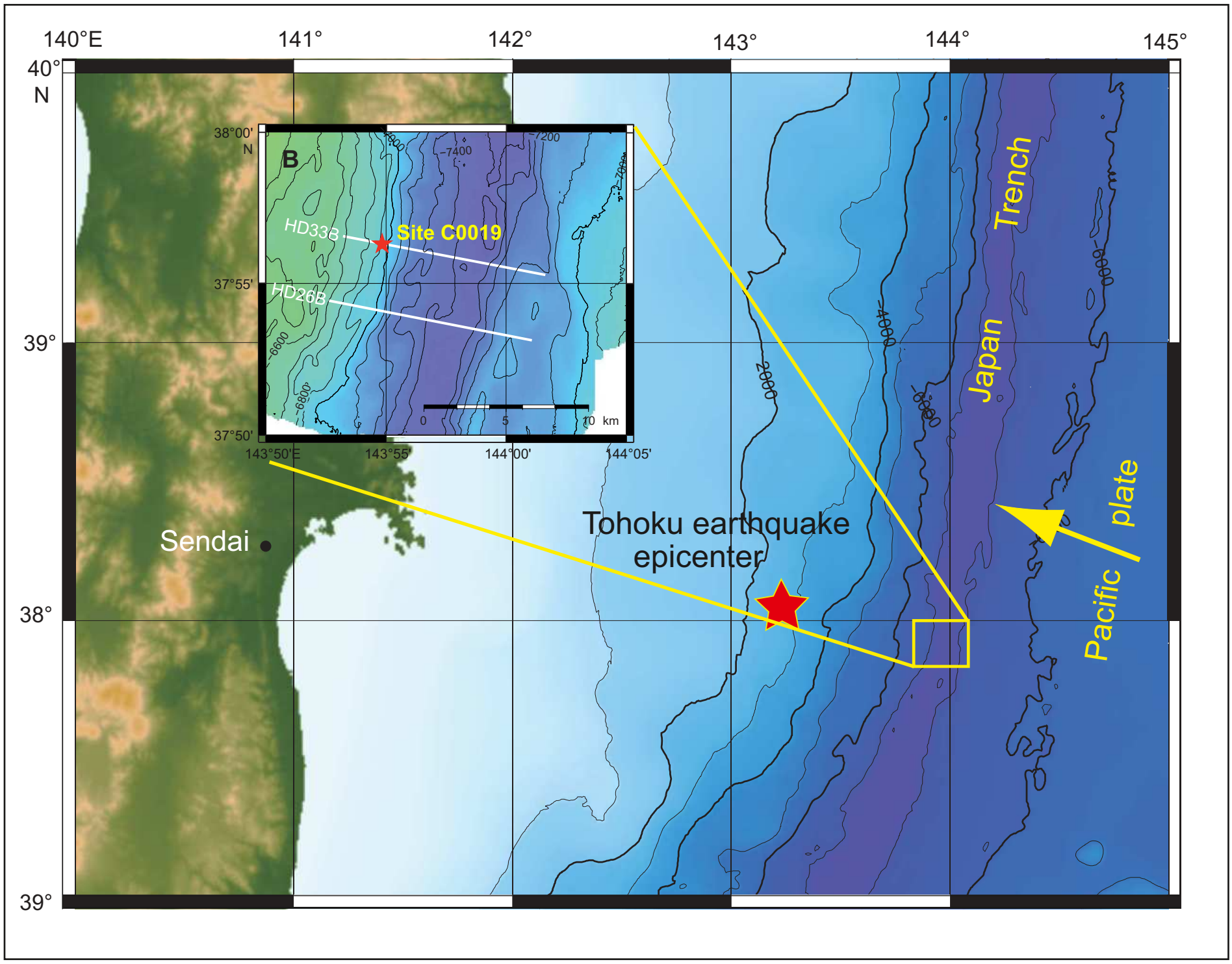
140°E
141°
142°
143°
144°
145°
40° N
39°
38°
38°00' N
37°55'
37°50'
143°50'E
143°55'
144°00'
144°05'
B
HD33B
Site C0019
HD26B
0
5
10 km
Sendai
Tohoku earthquake epicenter
Japan Trench
Pacific plate
-7200
-7400
-7600
-6600
-6800
-4000
-2000
-8000

a

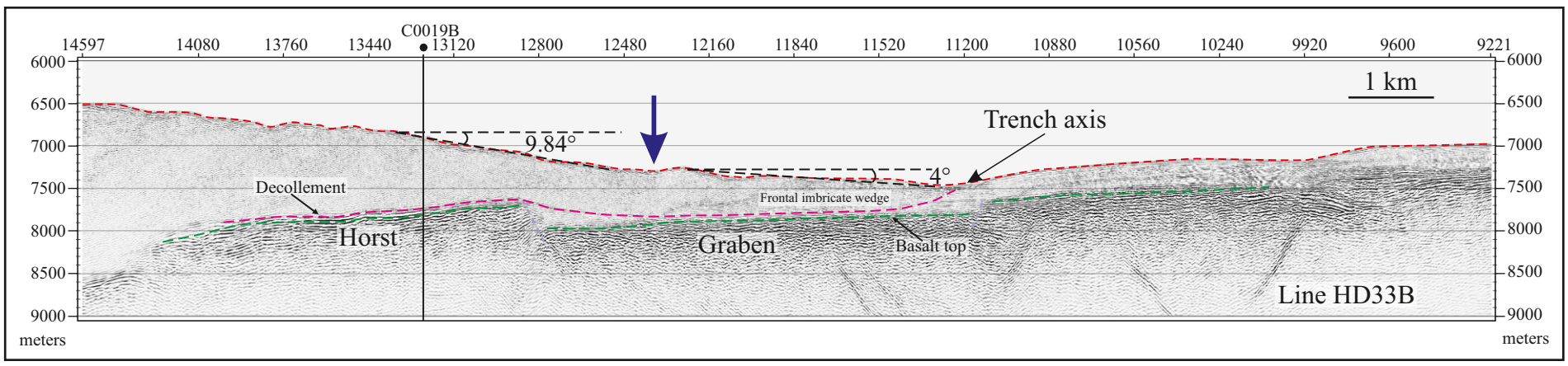
C0019B
14597
14080
13760
13440
13120
12800
12480
12160
11840
11520
11200
10880
10560
10240
9920
9600
9221
6000
6500
7000
7500
8000
8500
9000
meters
1 km
9.84°
4°
Trench axis
Decollement
Horst
Graben
Frontal imbricate wedge
Basalt top
Line HD33B

b

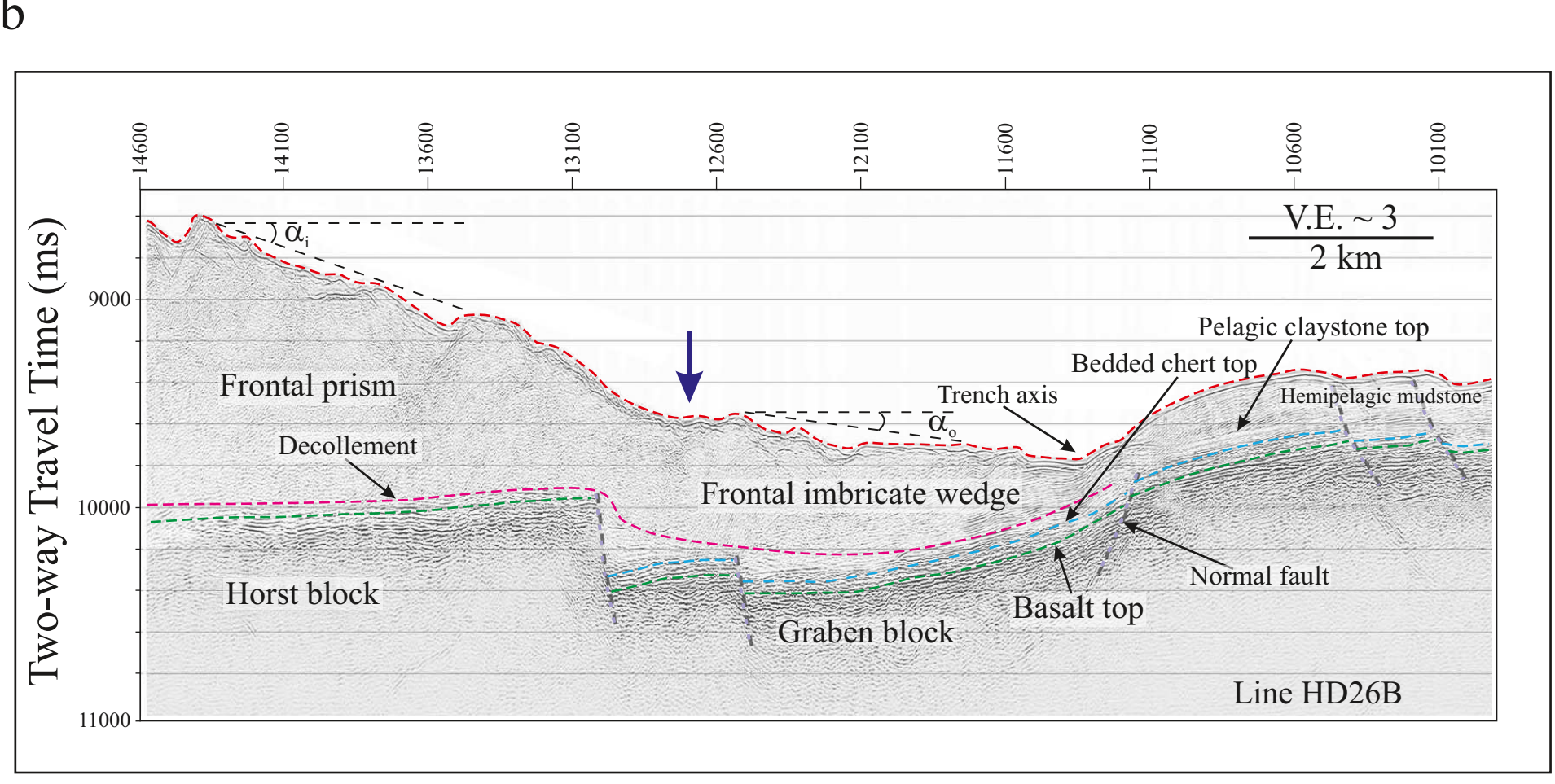
14600
14100
13600
13100
12600
12100
11600
11100
10600
10100
Two-way Travel Time (ms)
9000
10000
11000
V.E. ~ 3
2 km
αi
αo
Frontal prism
Decollement
Horst block
Graben block
Frontal imbricate wedge
Trench axis
Pelagic claystone top
Bedded chert top
Hemipelagic mudstone
Normal fault
Basalt top
Line HD26B

c

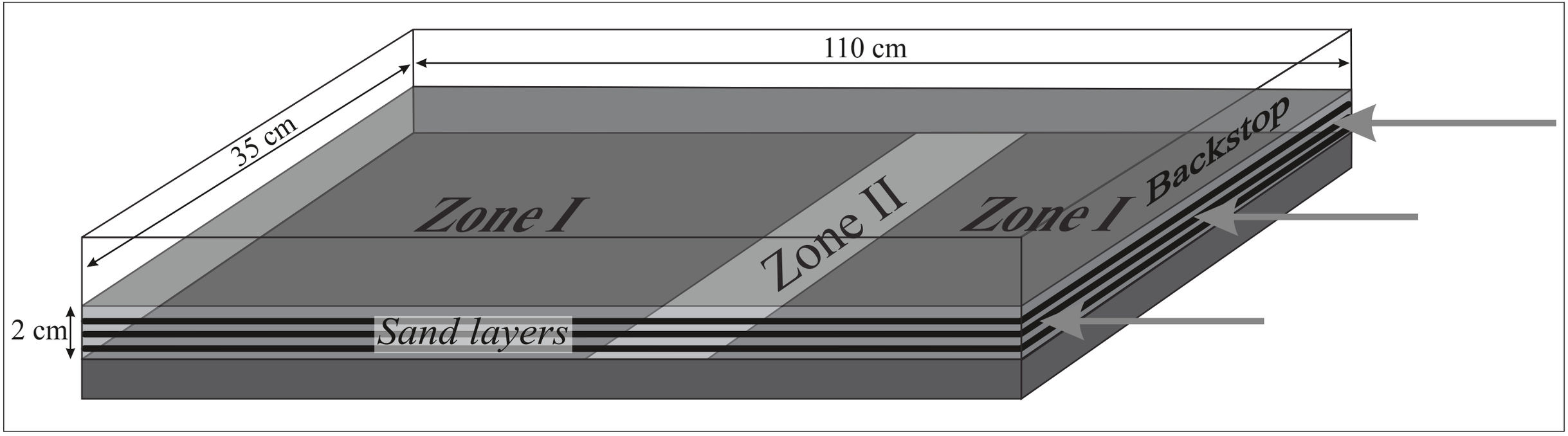
110 cm
35 cm
Zone I
Zone II
Zone I
Backstop
2 cm
Sand layers

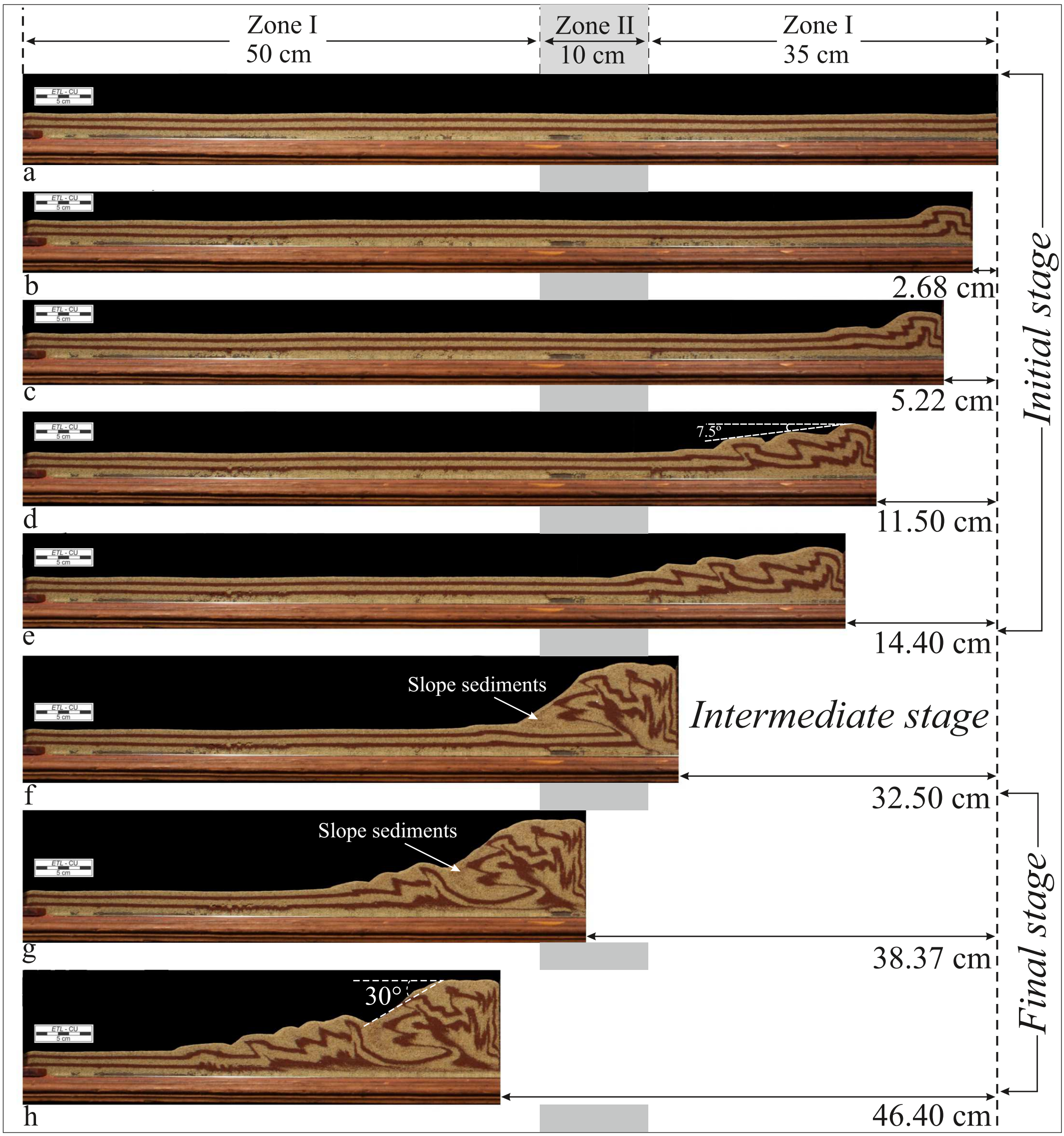
Zone I
50 cm
Zone II
10 cm
Zone I
35 cm
ETL - CU
5 cm
a
b
2.68 cm
c
5.22 cm
Initial stage
d
7.5°
11.50 cm
e
14.40 cm
f
Slope sediments
Intermediate stage
32.50 cm
g
Slope sediments
38.37 cm
Final stage
h
30°
46.40 cm

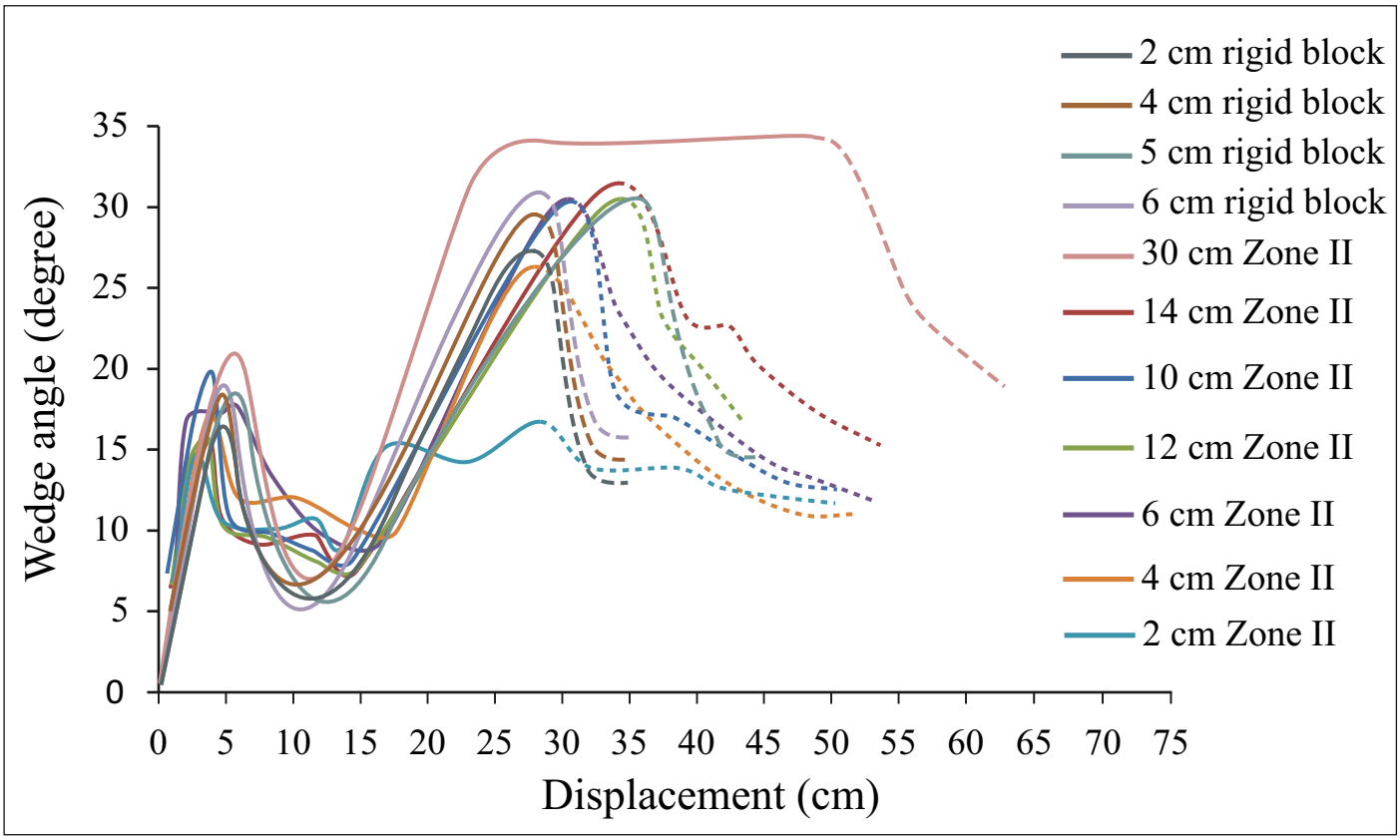
Wedge angle (degree)
0
5
10
15
20
25
30
35
0 5 10 15 20 25 30 35 40 45 50 55 60 65 70 75
Displacement (cm)
2 cm rigid block
4 cm rigid block
5 cm rigid block
6 cm rigid block
30 cm Zone II
14 cm Zone II
10 cm Zone II
12 cm Zone II
6 cm Zone II
4 cm Zone II
2 cm Zone II

a

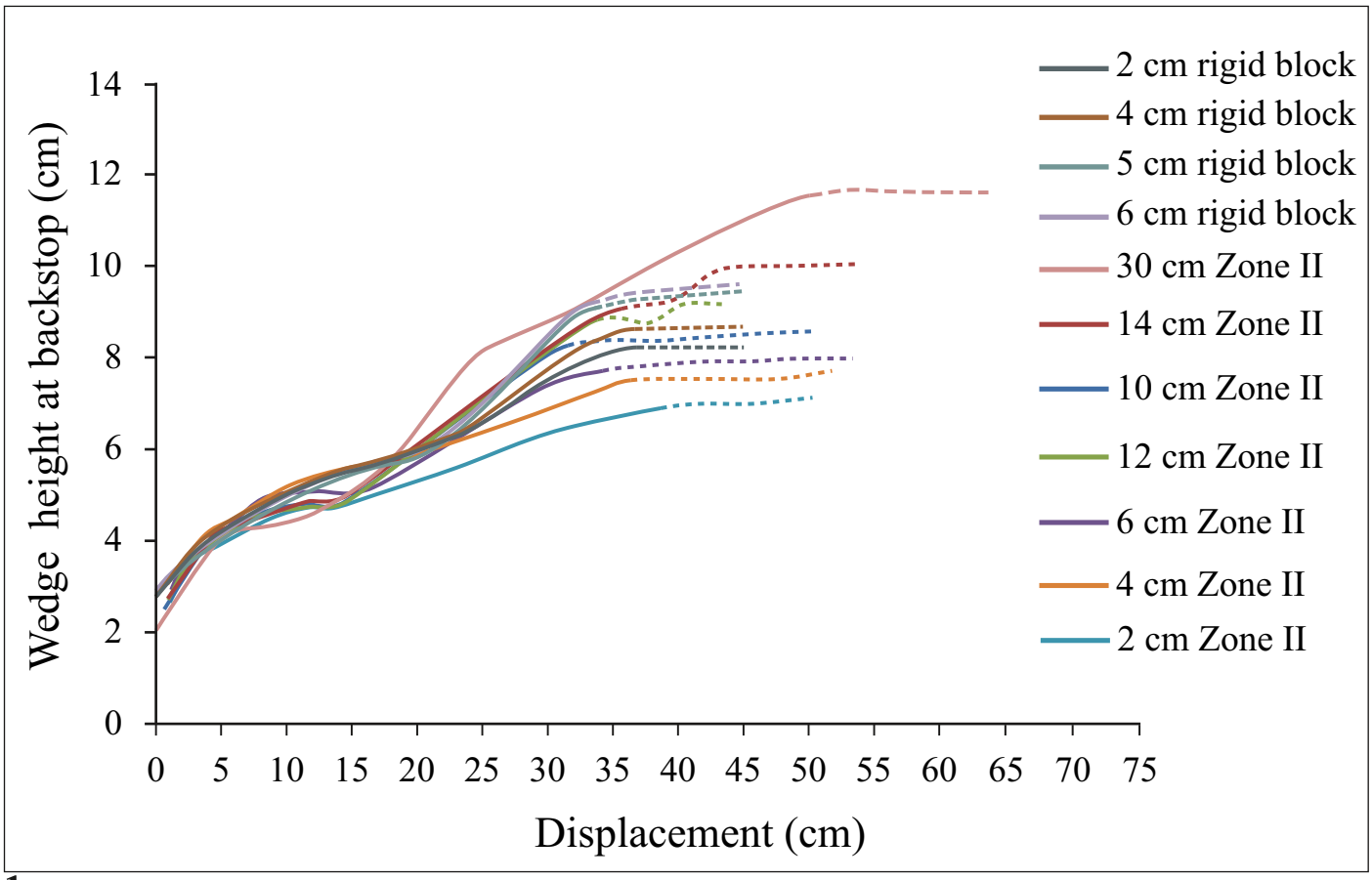
Wedge height at backstop (cm)
0
2
4
6
8
10
12
14
0 5 10 15 20 25 30 35 40 45 50 55 60 65 70 75
Displacement (cm)
2 cm rigid block
4 cm rigid block
5 cm rigid block
6 cm rigid block
30 cm Zone II
14 cm Zone II
10 cm Zone II
12 cm Zone II
6 cm Zone II
4 cm Zone II
2 cm Zone II

b

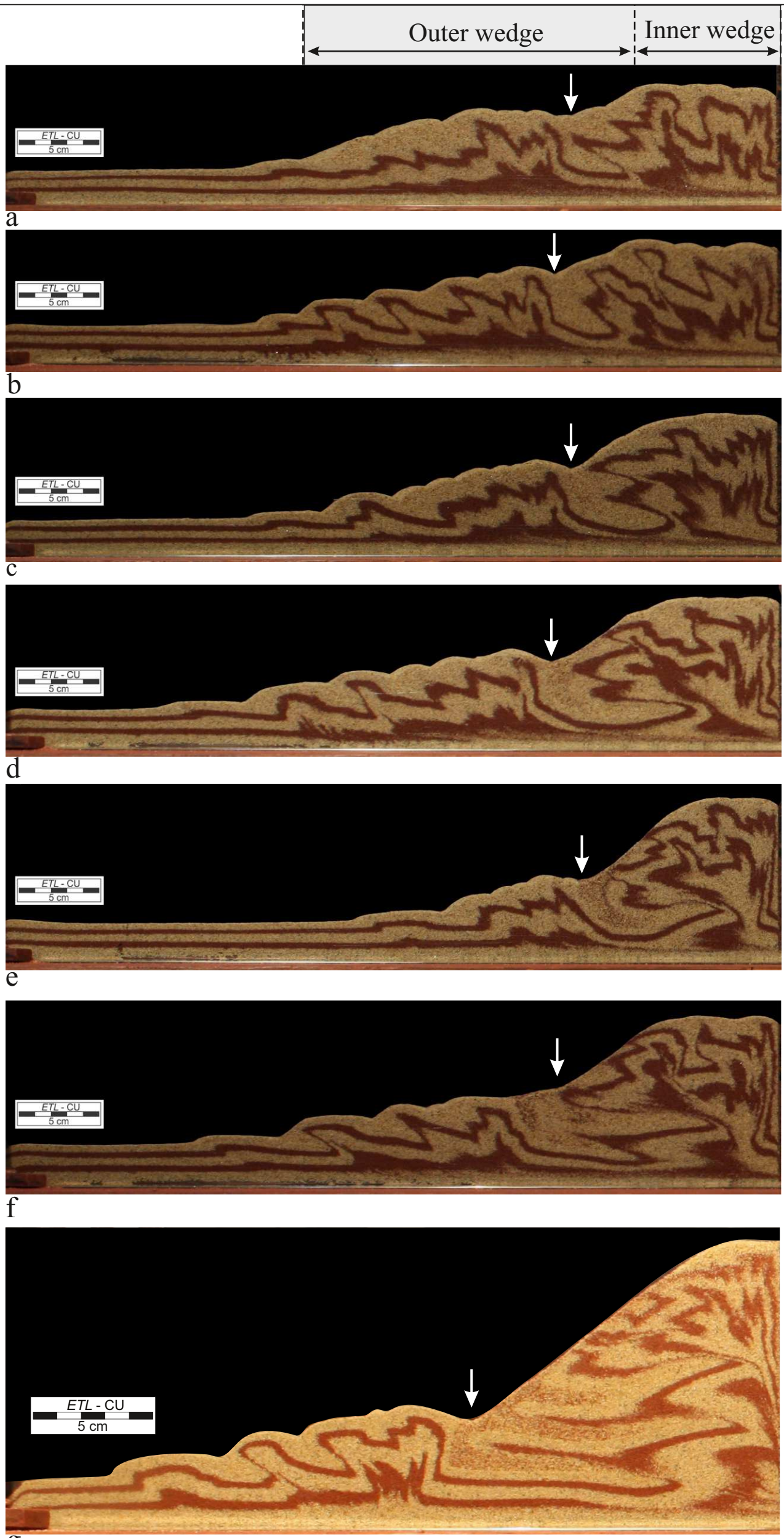
Outer wedge
Inner wedge
ETL - CU
5 cm
a
b
c
d
e
f
g

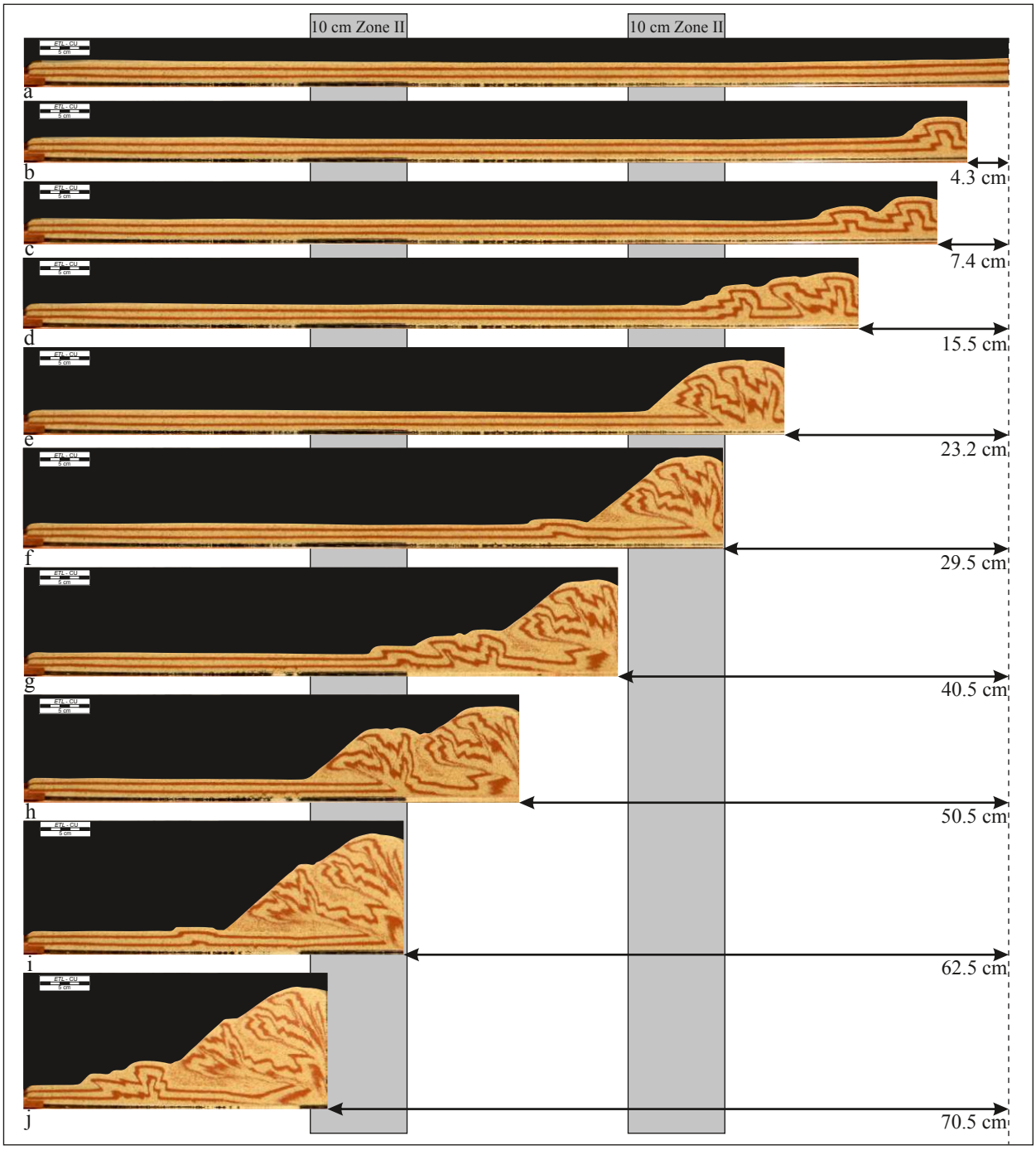
10 cm Zone II
10 cm Zone II
a
b
4.3 cm
c
7.4 cm
d
15.5 cm
e
23.2 cm
f
29.5 cm
g
40.5 cm
h
50.5 cm
i
62.5 cm
j
70.5 cm

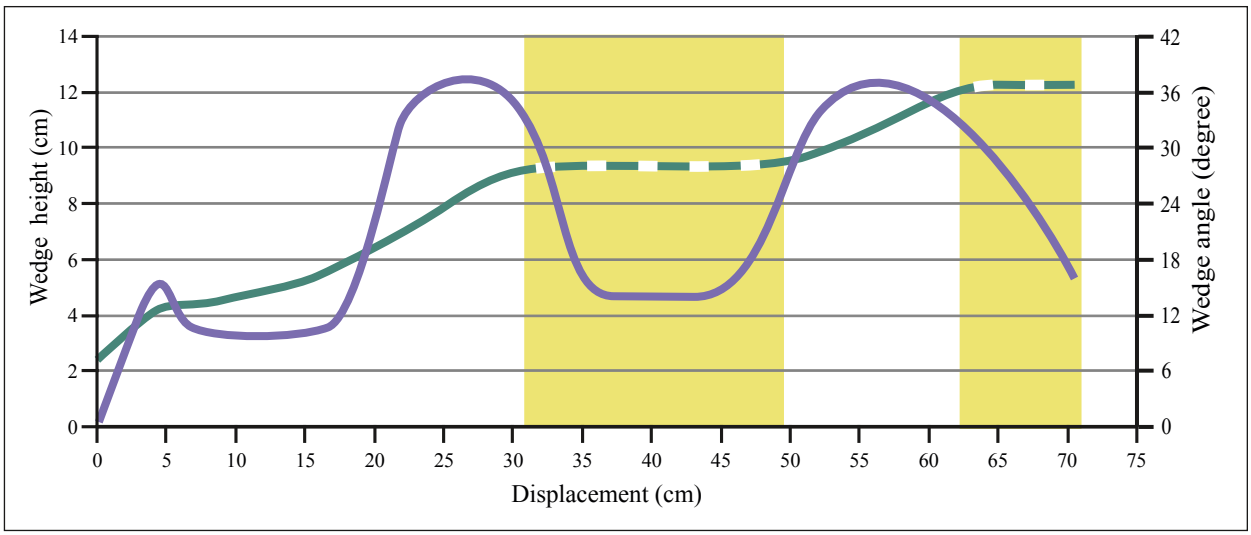
Wedge height (cm)
Wedge angle (degree)
Displacement (cm)
0
2
4
6
8
10
12
14
0
6
12
18
24
30
36
42
0
5
10
15
20
25
30
35
40
45
50
55
60
65
70
75

k

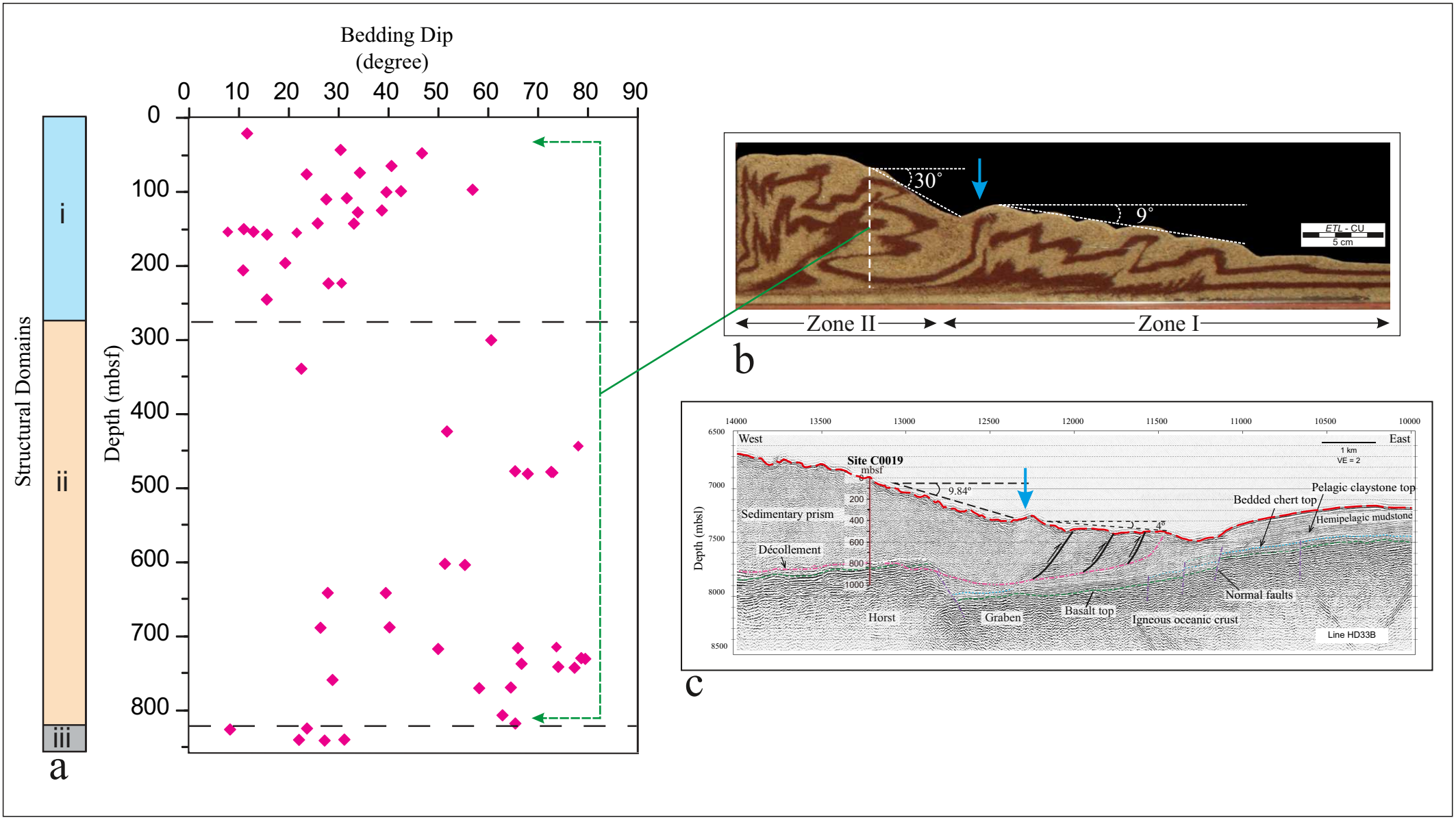
Bedding Dip
(degree)
0 10 20 30 40 50 60 70 80 90
0 100 200 300 400 500 600 700 800
Depth (mbsf)
Structural Domains
i
ii
iii
a
30°
9°
ETL - CU
5 cm
Zone II
Zone I
b
West
East
Site C0019
mbsf
9.84°
4°
1 km
VE = 2
Sedimentary prism
Décollement
Horst
Graben
Basalt top
Igneous oceanic crust
Normal faults
Bedded chert top
Pelagic claystone top
Hemipelagic mudstone
Line HD33B
Depth (mbsl)
14000 13500 13000 12500 12000 11500 11000 10500 10000
6500 7000 7500 8000 8500
200 400 600 800 1000
c